Journal of Radioanalytical and Nuclear Chemistry (2018) 318:1893–1900
https://doi.org/10.1007/s10967-018-6199-0

Measurement and covariance analysis of ^{232}Th(n, 2n)^{231}Th reaction cross sections at the effective neutron energies of 8.97 and 16.52 MeV

Meghna Karkera[1] · Haladhara Naik[2] · Sripathi Punchithaya[3] · Manjunatha Prasad[1] · Santhi Sheela Yeraguntla[1] · Saraswatula Venkata Suryanarayana[4] · Srinivasan Ganesan[5] · Vibha Vansola[6] · Rajnikanth Makhwana[6]

Received: 22 June 2018 / Published online: 5 October 2018

Abstract

The ^{232}Th(n, 2n)^{231}Th reaction cross sections relative to the ^{232}Th(n, f)^{97}Zr monitor reaction at the effective neutron energies of 8.97 and 16.52 MeV have been measured by using the activation and off-line γ-ray spectrometry. The neutron beams were generated from the ^{7}Li(p, n)^{7}Be reaction by using the proton beam energies of 11 and 18.8 MeV. Correction factors for the low energy neutrons were taken care by considering the thickness of sample and non mono-energetic neutrons. The covariance analysis in the uncertainty of the reaction cross section was carried out by using error propagation and micro-correlation technique. The present data were compared with the literature data, evaluated data and theoretical values based on TALYS-1.8 code.

Keywords ^{232}Th(n, 2n)^{231}Th reaction cross sections · ^{7}Li(p, n)^{7}Be reaction neutrons · Activation and off-line γ-ray spectrometry · Covariance analysis · TALYS-1.8 code

Introduction

India has a continuing programmatic interest in basic nuclear data science related to ^{232}Th–^{233}U fuel cycle [1]. This is because ^{232}Th–^{233}U fuel has a great potential to serve as a significant source of low carbon electricity in India. Thorium can also be utilized as a part of viable energy mix of options designed to last for several centuries. Developments of reactor design for the utilization of ^{232}Th–^{233}U fuel in the Advanced Heavy Water Reactor [2, 3] demands new nuclear data [4] for all the isotopes of ^{232}Th–^{233}U fuel cycle. As compared to ^{238}U and ^{239}Pu based fuels, the isotopes ^{232}Th and ^{233}U require several sequential captures of neutrons to form transactinide isotopes such as the isotopes of Pu, Am and Cm etc. Thus, the production of transactinide wastes in pure ^{232}Th–^{233}U based fuel is several orders of magnitude smaller than in ^{238}U–^{239}Pu based fuel. The ^{232}U nuclide of concern in fuel cycle is produced dominantly via the ^{232}Th(n, 2n) reaction route of thorium rods in thermal, fast, fusion and accelerator driven sub-critical systems (ADSs) [5]. A discussion of production routes of ^{232}U, and the important role of ^{232}U in ^{232}Th–^{233}U fuel cycle, and concerns, are discussed in the literature [6], and are not reproduced here to save space.

The experimental ^{232}Th(n, 2n)^{231}Th reaction cross sections data measured by various researchers within the neutron energies of 6–20 MeV are compiled in EXFOR library [7, 8]. Overall 102 data points are available in the literature during the time of writing this paper. These data show that the ^{232}Th(n, 2n)^{231}Th reaction cross-section increases from the threshold value and reaches a peak

✉ Haladhara Naik
naikhbarc@yahoo.com

1 Department of Statistics, Manipal Academy of Higher Education, Manipal 576104, India

2 Radiochemistry Division, Bhabha Atomic Research Center, Mumbai 400085, India

3 Department of Physics, National Institute of Engineering, Mysuru 570008, India

4 Nuclear Physics Division, Bhabha Atomic Research Center, Mumbai 400085, India

5 DAE, Bhabha Atomic Research Centre, Mumbai 400085, India

6 Maharaja Sayajirao University of Baroda, Vadodara 390002, India

around the neutron energy of 11 MeV. There after it decreases up to the neutron energy of 20 MeV [9–27].

In the present work, we measured the $^{232}Th(n,2n)^{231}Th$ reaction cross sections at the effective neutron energies of 8.97 and 16.52 MeV by using an activation method and off-line γ-ray spectrometric technique. We have used relative method, as described in Refs. [28, 29], where ^{97}Zr fission product from the ^{232}Th(n, f) reaction was taken as neutron flux monitor. We also present the covariance analysis of the experimental data by considering the partial uncertainties in various attributes and the correlations between those attributes. In Indian context, the covariance analysis of nuclear data presented in this paper are motivated by our programmatic interest [30]. More details on the data sets of the attributes used in the covariance analysis are available in the unpublished internal document [31] based on Refs. [28, 29] and are not reproduced here to save the space.

Experimental details

The experiment was carried out by using the 14 UD BARC-TIFR (Bhabha Atomic Research Centre-Tata Institute of Fundamental Research) Pelletron facility at Mumbai, India [32]. The neutron beam was produced by using the $^7Li(p,n)^7Be$ reaction with the proton beam energies of 11 and 18.8 MeV in the main line at 6 m above the analyzing magnet of the Pelletron facility to utilize maximum proton current from the accelerator. The incident proton current during the irradiation at 11 MeV and 18.8 MeV proton energies were 120 nA and 220 nA, respectively. A collimator of 6 mm diameter was used before the lithium target. The natural lithium foil of thickness 7.8 mg/cm^2 was sandwiched between two tantalum foils of different thicknesses. The front tantalum foil facing the proton beam was 3.2 mg/cm^2 thick. The degradation of proton energy according to SRIM code [32] due to Tantalum and Lithium foils were 39–56 keV and 78–276 keV, respectively. The back tantalum foil of thickness 41 mg/cm^2 was used to stop the proton beam. A schematic diagram of experimental setup used in the present irradiations is shown in Fig. 1.

The neutron energy (E_n) due to the $^7Li(p,n)^7Be$ reaction was obtained by using the kinematic relation $E_n = E_P - E_{Th}$. E_P and E_{th} are the incident proton energy and the threshold energy of the $^7Li(p,n)^7Be$ reaction. For the proton beams of energy higher than 2.4 MeV, the emerging neutrons are not mono-energetic due to the excited states of beryllium. Thus, the effective neutron energy for each of the two proton energies is obtained by taking the average of the one given by the kinematic relation and the other given by considering the primary group of neutrons in the neutron spectra taken from Refs. [33, 34]. By considering the errors in the neutron energy obtained by kinematic relation and based on the neutron spectrum, the error in the effective neutron energy was propagated. The details of computation are given in the internal document [31] based on Refs. [20, 28]. The respective effective neutron energies with reference to the proton energies of 11 and 18.8 MeV are found to be 8.97 ± 0.34 and 16.52 ± 0.30 MeV, respectively.

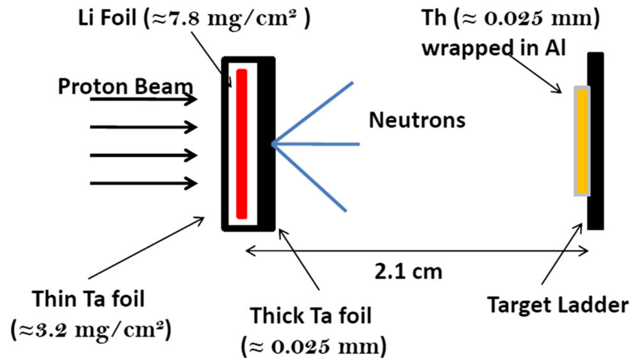

Fig. 1 A schematic diagram of experimental setup used for the irradiations

Two thorium metal foils of purity more than 99.99.99% weighing 0.9005 ± 0.0003 and 0.3955 ± 0.0003 g were wrapped with aluminum foils of thickness 0.025 mm to prevent radioactive contamination from the samples to surrounding. The aluminum wrapped thorium samples were then mounted one at a time at an angle of 0° with respect to the proton beam's direction at a distance of 2.1 cm behind the Ta–Li–Ta stack. The stacks in sequence were irradiated one at a time with effective neutron energies of 8.97 and 16.52 MeV for the duration of 16.08 and 5 h, respectively. The irradiated foils of thorium from two stacks were then cooled for 34.96 and 69.1 h, respectively and then mounted separately on different Perspex plates. The fission product, ^{97}Zr produced in the ^{232}Th(n, f) reaction was used as neutron flux monitor in both the irradiations.

Gamma ray counting of the irradiated foils was performed by using a pre-calibrated 80-cc High Purity Germanium detector coupled to a PC-based 4096 channel analyzer. The counting dead time was always kept lesser than 5% by placing the irradiated thorium samples at a distance of 1 cm from the end cap of the detector. The energy and efficiency calibration of the detector system were performed by using standard ^{133}Ba and ^{152}Eu sources, keeping the same geometry. The details of calibration and model detection are provided in the unpublished internal document [31] based on Refs. [28, 29].

Data analysis and results

In the present work, the cross sections of $^{232}Th(n,2n)^{231}Th$ reaction at the effective neutron energies of 8.97 and 16.52 MeV were measured by using the following equation.

$$\sigma_U = \sigma_M.Y.\frac{C_U\lambda_U Wt_M abn_M Av_U (I_\gamma)_M \varepsilon_{\gamma(M)}\left(1-e^{-\lambda_m t_{irr_M}}\right)\left(e^{-\lambda_M t_{cool_M}}\right)\left(1-e^{-\lambda_M t_{C_M}}\right)}{C_M\lambda_M Wt_U abn_U Av_M (I_\gamma)_U \varepsilon_{\gamma(U)}\left(1-e^{-\lambda_U t_{irr_U}}\right)\left(e^{-\lambda_U t_{cool_U}}\right)\left(1-e^{-\lambda_U t_{C_U}}\right)}\prod_k\frac{(C_k)_M}{(C_k)_U} \quad (1)$$

where $\sigma_U(E_n)$ and $\sigma_M(E_n)$ denote cross section of $^{232}Th(n,2n)^{231}Th$ reaction and cross section of the $^{232}Th(n,f)$ reaction at the neutron energy E_n, respectively, Y denotes yield of ^{97}Zr fission product in the $^{232}Th(n,f)$ reaction, C_U and C_M denotes the detected γ-ray peak counts of the reaction product ^{231}Th and fission product ^{97}Zr, respectively, λ_U, λ_M denote decay constants of the product nuclides ^{231}Th and ^{97}Zr, respectively, $\varepsilon_{\gamma(U)}, \varepsilon_{\gamma(M)}$ denote efficiency of detector corresponding to characteristic γ-rays of the product nuclides ^{231}Th and ^{97}Zr, respectively, Wt_U and Wt_M are the same and denote weights of ^{232}Th, abn_U and abn_M are the same and denote isotopic abundances of the ^{232}Th, Av_U, Av_M are the same and denote average atomic mass of ^{232}Th, $(I_\gamma)_U$ and $(I_\gamma)_M$ denote γ-ray abundances of the ^{231}Th and ^{97}Zr. t_{irr}, t_{cool} and t_c denote the irradiation time, cooling time and counting time of the samples. $(C_k)_U$ and $(C_k)_M$ denote the correction factors of sample and monitor reactions, respectively for the kth attribute, where k represents the dead time of the detector $\left(\frac{\text{Clocktime}}{\text{Live time}}\right)$, low energy neutron contribution (α) and γ-ray self-attenuation factor (Γ_{attn}). The correction term, α is obtained following the approach given originally by Smith et al. [35] and used in our team's earlier work by Shivashankar et al. [28] and Yerraguntla et al. [29]. It may be noted that

$$\alpha_i = \left(1+\frac{\sum_{p_2}\Phi(E_{P_2})\sigma_i(E_{P_2})+\int_0^{E_{max}}\varphi(E)\sigma_i dE}{\sum_{p_1}\Phi(E_{P_1})\sigma_i(E_{P_1})}\right), \quad i=U,M \quad (2)$$

where Φ represents the flux corresponding to discrete peaks, and φ is the continuum with reference to the neutron spectra. E_{P_1}, E_{P_2} represent the neutron energies corresponding to higher and lower energy neutron peaks. E corresponds to much lower energy tail part of the neutron spectra. The self-attenuation factor $(\Gamma_{attn})_i; i=U,M;$ of the foils were determined by using the expression, $\Gamma_{attn}=\frac{1-e^{-\mu l}}{\mu l}$, where l is the thickness of the sample and μ is mass attenuation coefficient obtained from XMuDat Ver. 101 [36, 37].

Efficiency calibration, model detection and estimation of efficiency of HPGe detector

Standard point sources of ^{133}Ba and ^{152}Eu were used for energy-efficiency calibration and placed at a distance of 1 cm from the end cap of the High Purity Germanium Detector. The efficiencies corresponding to the characteristic γ-ray energies of ^{133}Ba and ^{152}Eu were obtained by using the following equation.

$$\varepsilon_\gamma = \frac{CK_c}{A_o a e^{\frac{-0.693t}{t_{1/2}}}} \quad (3)$$

where ε_γ, C, K_c, a, A_o, $t_{1/2}$ and t denotes efficiency of the detector, detected γ-ray counts under the photo-peak per second, correction factor for the coincidence summing effect, branching factor or γ-ray abundance, activity at the time of source calibration, half-life of radioactive nuclide, time elapsed between calibration at the time of packing and at the time of the experiment.

The experimental data (C), simulated data (K_c) and auxiliary data A_o, a and $t_{1/2}$ at 11 gamma lines of ^{133}Ba and ^{152}Eu are presented in Table 1. The counts C was obtained by using γ-ray spectrometry. Counting time for ^{133}Ba and ^{152}Eu standard sources were 1500 and 2400 s, respectively. The coincidence summing correction factor (K_c) was obtained by using the Monte Carlo simulation code EFFTRAN [38]. The data for A_o was supplied by the manufacturer. The decay data for γ-ray abundance and half-life were taken from NuDat [39].

Using the uncertainty data for C, A_o, a and $t_{1/2}$ and ascribing micro-correlations between them the covariance matrix V_ε for 11 observations was propagated. We further obtain linear parametric function $\ln\varepsilon = 4.03 - 0.90(\ln E) + 0.16(\ln E)^2 - 0.04(\ln E)^3 - 0.068(\ln E)^4$ as energy-efficiency model with $\frac{\chi^2}{11-5}$ = 1.72 (nearest to 1

Table 1 Efficiency calibration data of detector using standard sources ^{133}Ba and ^{152}Eu

Gamma-ray energy (keV)	Gamma-ray abundance a (%)	Counts	Half-life (y)	K_C	Efficiency
^{152}Eu					
121.8	28.53 ± 0.16	240,401 ± 900	13.517 ± 0.014	1.118	0.1171
488.7	0.414 ± 0.003	984 ± 104		1.222	0.0361
688.7	0.856 ± 0.006	1742 ± 119		1.053	0.0266
778.9	12.93 ± 0.08	20,775 ± 197		1.112	0.0222
964.1	14.51 ± 0.07	19,723 ± 192		1.092	0.0184
1408.0	20.87 ± 0.09	20,700 ± 154		1.072	0.0132
^{133}Ba					
53.2	2.14 ± 0.03	2287 ± 231	10.551 ± 0.011	1.155	0.0173
81.0	32.9 ± 0.30	220,630 ± 822		1.124	0.1055
223.2	0.453 ± 0.003	2326 ± 166		1.096	0.0788
276.4	7.16 ± 0.05	31,041 ± 227		1.091	0.0662
302.9	18.34 ± 0.13	76,396 ± 208		1.048	0.0611
356.0	62.05 ± 0.19	221,606 ± 498		1.039	0.0520
383.8	8.94 ± 0.06	32,705 ± 201		0.910	0.0466

Table 2 Interpolated detector efficiencies

Radionuclide	γ-ray energy (keV)	Efficiency (ε_γ)	Correlation matrix	
^{231}Th	84.2	0.062 ± 0.0040	1	
^{97}Zr	743.3	0.023 ± 0.00028	0.15	1

among all those $\frac{\chi^2}{df}$ obtained for different models considered with different linear parametric functions). For more details on covariance analysis and model detection, refer to Refs. [28, 29, 31]. Further, the efficiency of detector at characteristic γ-ray energy corresponds to ^{231}Th and ^{97}Zr (84.2 and 743.3 keV, respectively) were obtained by interpolation technique, whereas the covariance information for these measurements was obtained by propagation technique. We present the relevant data in Table 2.

Estimation of ^{232}Th(n, 2n)^{231}Th reaction cross section with covariance analysis

Among the attributes mentioned in Eq. (1), the attributes measured with error are $\sigma_M(E_n)$, C_U, C_M, λ_U, λ_M, Av_M, Av_U, Wt_U, Wt_M, $(I_\gamma)_U$, $(I_\gamma)_m$, $\varepsilon_{\gamma(U)}$, $\varepsilon_{\gamma(M)}$, $(\Gamma_{\mathrm{attn}})_U$, $(\Gamma_{\mathrm{attn}})_M$, Y. Other attributes namely, t_{irr}, t_{cool} and t_c given in Eq. (1)

Table 3 Decay data of radio-nuclides required for estimating $\sigma_U(E_n)$

Isotope	Half-life (h)	γ-ray abundance	Isotopic abundance
^{97}Zr	16.749 ± 0.008	0.9309 ± 0.0016	1
^{231}Th	24.52 ± 0.01	0.066 ± 0.004	

are observed without error and treated as constants. Basic decay data of the attributes required to determine cross section are presented in Table 3. The data for yields with error (0.049195 ± 0.003955 and 0.04495 ± 0.004186) were taken from Refs. [40–42].

The cross sections for the $^{232}\mathrm{Th(n, f)}$ reaction was obtained from ENDF/B-V111.0 and then interpolated to obtain cross section at neutron energies of our interests, namely, 8.97 and 16.52 MeV. The data with necessary covariance information is given Table 4.

The cross sections of $^{232}\mathrm{Th(n, 2n)}^{231}\mathrm{Th}$ reaction at the neutron energies of 8.97 and 16.52 MeV were obtained by substituting the basic data of the attributes in Eq. (1) and presented in Table 6. The covariance matrix associated with these two measurements are obtained by considering the observations of all the attributes and their covariance information. The covariance matrix V_{σ_U} is given by

$$(V_{\sigma_U})_{ij} = \sum_{\mathrm{kl}} (e_k)_i (e_l)_j (s_{kl})_{ij}, \quad 1 \le i,\ j \le 2,\ 1 \le l,\ k \le 16 \tag{4}$$

where σ_{Ui} is a vector consisting of two entries with the measurements of $^{232}\mathrm{Th(n, 2n)}^{231}\mathrm{Th}$ reaction cross sections at the neutron energies of 8.97 and 16.52 MeV

$(e_k)_i = \frac{\partial \sigma_{Ui}}{\partial (x_k)_i} \Delta(x_k)_i$ is the partial uncertainty in σ_{Ui} due to the k th attribute amongst the list given above, $(\boldsymbol{e_k})_{\boldsymbol{j}} =$

Table 4 ^{232}Th(n, f) reaction cross sections at the neutron energies

Neutron energy (MeV)	^{232}Th(n, f) reaction cross section (barn)	Correlation matrix	
8.97 ± 0.34	0.3370 ± 0.0073	1	
16.52 ± 0.30	0.4613 ± 0.0105	0.89	1

Table 5 Partial uncertainties in the ^{232}Th(n, 2n)^{231}Th reaction cross section

Attributes	E_n = 8.97 MeV	E_n = 16.52 MeV	Correlation
Photo-peak counts of gamma-ray C_U	4.46E-02 (2.4%)	1.98E-02 (3.2%)	Uncorrelated
Decay constant λ_U	1.17E-04 (6.4E-03%)	2.32E-04 (3.7E-02%)	Fully correlated
Average atomic mass Av_U	1.20E-08 (6.6E-07%)	4.07E-09 (6.6E-07%)	Fully correlated
Weight of the sample Wt_U	5.86E-04 (3.2E-02%)	4.53E-04 (7.3E-02%)	Uncorrelated
Gamma ray abundance $(I_\gamma)_U$	1.11E-01 (6.1%)	3.76E-02 (6.1%)	Fully correlated
Efficiency of detector $\varepsilon_{\gamma(U)}$	1.20E-01 (6.6%)	4.06E-02 (6.6%)	Fully correlated
^{232}Th(n, f) reaction cross section	3.97E-02 (2.2%)	1.41E-02 (2.3%)	Partially correlated[a]
Yield Y	1.47E-01 (8.0%)	5.78E-02 (9.3%)	Uncorrelated
Gamma attenuation coefficient $(\Gamma_{\mathrm{attn}})_M$	1.36E-03 (7.4E-02%)	7.10E-04 (1.1E-01%)	Uncorrelated
Photo-peak counts of gamma-ray C_M	1.29E-01 (7.1%)	5.69E-02 (9.2%)	Uncorrelated
Decay constant λ_M	6.64E-04 (3.6E-02%)	5.86E-04 (9.4E-02%)	Fully correlated
Average atomic mass Av_M	1.20E-08 (6.6E-07%)	4.07E-09 (6.6E-07%)	Fully correlated
Weight of sample Wt_M	5.86E-04 (3.2E-02%)	4.53E-04 (7.3E-02%)	Uncorrelated
Gamma ray abundance $(I_\gamma)_M$	3.14E-03 (1.7E-01%)	1.07E-03 (1.7E-01%)	Fully correlated
Efficiency of detector $\varepsilon_{\gamma(M)}$	2.19E-02 (1.2%)	7.45E-03 (1.2%)	Fully correlated
Gamma attenuation coefficient $(\Gamma_{\mathrm{attn}})_U$	2.70E-02 (1.5%)	1.22E-02 (2.0%)	Uncorrelated

[a]Correlation value is given Table 4

$\frac{\partial \sigma_{Uj}}{\partial (x_k)_j} \Delta (x_k)_j$ is the partial uncertainty in σ_{Uj} due to the l th attribute amongst the list given above, $(s_{kl})_{ij}$ is the micro-correlation between i th observation due k th attribute and j th observation l th attribute. For the detailed derivation of Eq. (4) with necessary description, the readers can referred to reference by Santhi Sheela et al. [43]. The partial uncertainties in σ_U due to each of the sixteen attributes appearing in Eq. (1) are obtained as in the description of Eq. (4) and the same is presented in Table 5.

The observations between any pair attributes appearing in Eq. (1) are independent of each other except for the pairs of attributes $(\varepsilon_{\gamma(U)}, \varepsilon_{\gamma(M)})$, $(\mathbf{Av_U}, \mathbf{Av_M})$ and $(\mathbf{Wt_U}, \mathbf{Wt_m})$ respectively, where $\mathrm{cor}(\varepsilon_{\gamma(U)}, \varepsilon_{\gamma(M)}) = 0.1452$, $\mathrm{cor}(\mathbf{Av_U}, \mathbf{Av_M}) = 1$ and in the case of the attribute $\mathbf{Wt}$ and at given neutron energy, the correlation between the observation of $\mathbf{Wt_U}$, and the observation of $\mathbf{Wt_M}$ is one. The observations of attributes $\mathbf{C_U}, \mathbf{C_M}$, $\mathbf{Wt_U}$, $\mathbf{Wt_M}$, $(\boldsymbol{\Gamma}_{\mathbf{attn}})_\mathbf{U}$, $(\boldsymbol{\Gamma}_{\mathbf{attn}})_\mathbf{M}$, and $\mathbf{Y}$ with reference to different neutron energies are independent, therefore the corresponding micro-correlation matrices are identity matrices of size two. For each of the attributes $\boldsymbol{\lambda}_\mathbf{U}$, $\boldsymbol{\lambda}_\mathbf{M}$, $\mathbf{Av_M}$, $\mathbf{Av_U}$, $(\mathbf{I}_\gamma)_\mathbf{U}$, $(\mathbf{I}_\gamma)_\mathbf{M}$, $\varepsilon_{\gamma(U)}$, $\varepsilon_{\gamma(M)}$ the micro-correlation matrices for observation correspond to sample and observation correspond to monitor are identical and equal to $\boldsymbol{J}$ matrix of order 2 with all entries equal to one. Table 6 presents the covariance matrix of $\boldsymbol{\sigma}_\mathbf{U}$.

Discussion

In the present study, the cross sections of ^{232}Th(n, 2n)^{231}Th reaction were measured relative to the ^{232}Th(n, f)^{97}Zr monitor reaction at the effective neutron energies of 8.97 and 16.52 MeV by using activation and off-line γ-ray

Table 6 Experimentally measured ^{232}Th(n, 2n)^{231}Th reaction cross sections with correlation matrix

Neutron energy (MeV)	^{232}Th(n, 2n)^{231}Th reaction cross section (barn)	Correlation matrix	
8.97 ± 0.34	1.82 ± 0.27	1	
16.52 ± 0.30	0.62 ± 0.10	0.37	1

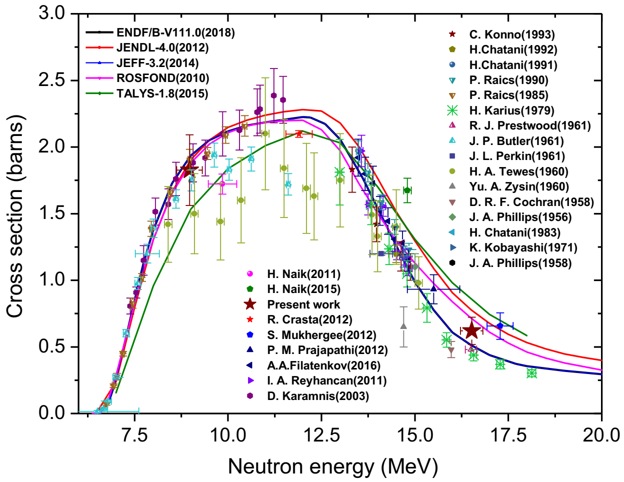

Fig. 2 Comparison of experimental ^{232}Th(n, 2n) reaction cross sections with the evaluated data from different libraries and theoretical values from TALYS-1.8

spectrometric technique. For comparison, we present our current data in Fig. 2 along with other data available in the literature [9–27] from EXFOR [7, 8]. In the same figure, we have also plotted the evaluated data curves from the ENDF/B-VIII.0 [44], JENDL 4.0 [45], JEFF-3.2 [46] and ROSFOND [47] libraries. It can be seen from Fig. 2 that our measurements of the ^{232}Th(n, 2n)^{231}Th reaction cross section at the neutron energy of 8.97 MeV is found to be in good agreement with all the evaluated data from different libraries [44–47]. However, the measurement at the neutron energy of 16.52 MeV is in between the evaluated curves given by ENDF/B-VIII.0 [44], which coincides with JEFF-3.2 and the rest [45–47].

Further, Fig. 2 shows that within the neutron energies of 9–13 MeV, there are large variations among the literature data [9–27]. Some of the literature data are significantly lower than the evaluated data of different libraries [44–47]. In view of this, the ^{232}Th(n, 2n)^{231}Th reaction cross section was theoretically calculated by using the TALYS-1.8 code [48]. TALYS is a computer code [48], which can be used to calculate the reaction cross-section based on physics models and parameterizations. It calculates nuclear reactions involving targets with mass larger than 12 amu and projectiles like photon, neutron, proton, ^{2}H, ^{3}H, ^{3}He and alpha particles in the energy range from 1 keV to 200 MeV. In the present work, we have used neutron as a projectile and ^{232}Th as a target. We have used the neutron energy from the threshold value of ^{232}Th(n, 2n)^{231}Th reaction (i.e. 6.4682 MeV) up to 20 MeV. The calculation of ^{232}Th(n, 2n) reaction cross-section was done by using the default parameters. Theoretically calculated ^{232}Th(n, 2n)^{231}Th reaction cross sections are plotted in Fig. 2.

It can be seen from Fig. 2 that the curve from TALYS follows a similar trend of experimental data and evaluated data. However, there is a right shift of the theoretical values compared to the evaluated data. Thus within the neutron energies of 9–13 MeV, the values from TALYS are passing through the middle of scattered experimental data. Below the neutron energies of 13 MeV, the data from TALYS are lower than the evaluated data. On the other hand, it is slightly higher than the evaluated data above the neutron energy of 15 MeV. In spite of these differences, a general increase trend of ^{232}Th(n, 2n)^{231}Th reaction cross-section from the threshold values to a maximum value around the neutron energy of 11–13 MeV is clearly seen for theoretical and evaluated data. However, the experimental data around the neutron energies of 11–13 MeV are very much limited and are lower than both the theoretical and evaluated data, which suggest the experimentalist for its redetermination. Above the, neutron energy of 13 MeV, the (n, 2n) reaction cross-section of ^{232}Th decreases due to the opening of other reaction channels, which indicates the shearing of energy in different channels.

Conclusion

The ^{232}Th(n, 2n)^{231}Th reaction cross sections relative to the ^{232}Th(n, f)^{97}Zr monitor reaction at the average neutron energies of 8.97 and 16.52 MeV have been measured by using the activation and off-line γ-ray spectrometric technique. The neutron beams were generated from the ^{7}Li(p, n)^{7}Be reaction by using the proton beam energies of 11 and 18.8 MeV. Correction factor accounting for low energy neutrons were used for the measurement by considering the thickness of sample and non mono-energetic neutrons from the accelerator. The efficiency of detector was determined by using ^{152}Eu and ^{133}Ba standard sources after taking care of coincidence summing effect. Least square method was employed to obtain the energy-efficiency model and γ-ray self-attenuation correction. The uncertainties of all the attributes for the cross section were taken care except the time factor. The covariance analysis in the uncertainty of the reaction cross section was carried out by using error propagation and micro-correlation technique. The ^{232}Th(n, 2n)^{231}Th reaction cross section as a function of neutron energy was also theoretically calculated by using TALYS-1.8 code with default parameters. The present data were compared with the literature data, evaluated data of ENDF/B-VIII.0, JENDL 4.0, JEFF-3.2 and ROSFOND libraries as well as with the theoretical values from TALYS-1.8 code and found to be in general agreement.

Acknowledgements The research work was supported by DAE-BRNS project (Sanction No. 36(6)/14/52/2014-BRNS/2708). The authors would like to thank the staff of BARC-TIFR Pelletron facility for their kind co-operation in providing the proton beam to carry out the experiment.

References

1. Ganesan S (2016) Nuclear data development related to the Th–U fuel cycle in India. In: Thorium energy for the world. Springer, Cham, pp 199–206
2. Sinha RK, Kakodkar A (2006) Design and development of the AHWR—the Indian thorium fuelled innovative nuclear reactor. Nucl Eng Des 236(7–8):683–700
3. DAE website (2018) A brochure "Advanced heavy water reactor". http://dae.nic.in/writereaddata/.pdf_37. Accessed Sept 2008
4. Ganesan S (2005) New reactor concepts and new nuclear data needed to develop them. In: AIP conference proceedings, vol. 769(1). AIP, pp 1411–1416
5. Ganesan S (2007) Nuclear data requirements for accelerator driven sub-critical systems—a roadmap in the Indian context. Pramana 68(2):257–268
6. Ganesan S, Sharma AR, Wienke H (2002) New investigations of the criticality property of pure ^{232}U. Ann Nucl Energy 29(9):1085–1104
7. IAEA-EXFOR Database available at http://www-nds.iaea.org/exfor
8. Otuka N, Dupont E, Semkova V, Pritychenko B, Blokhin AI, Aikawa M, Babykina S, Bossant M, Chen G, Dunaeva S, Forrest RA, Fukahori T, Furutachi N, Ganesan S, Ge Z, Gritzay OO, Herman M, Hlavac S, Kato K, Lalremruata B, Lee YO, Makinaga A, Matsumoto K, Mikhaylyukova M, Pikulina G, Pronyaev VG, Saxena A, Schwerer O, Simakov SP, Soppera N, Suzuki R, Takacs S, Tao X, Taova S, Raykanyi F, Varlamov VV, Wang J, Yang SC, Zerkin V, Zhuang Y (2014) Towards a more complete and accurate experimental nuclear reaction data library (EXFOR): international collboration between Nuclear Reaction Data Centres (NRDC). Nucl Data Sheets 120:272–276
9. Naik H, Prajapati PM, Surayanarayana SV, Jagadeesan KC, Thakare SV, Raj D, Mulik VK, Sivashankar BS, Nayak BK, Sharma SC, Mukherjee S, Singh S, Goswami A, Ganesan S, Manchanda VK (2011) Measurement of the neutron reaction cross-section of ^{232}Th using the neutron activation technique. Eur Phys J A 47:51
10. Prajapati PM, Naik H, Suryanarayana SV, Mukherjee S, Jagadeesan KC, Sharma SC, Goswami A (2012) Measurement of the neutron capture cross-sections of ^{232}Th at 5.9 MeV and 15.5 MeV. Eur Phys J A 48(3):35
11. Crasta R, Naik H, Suryanarayana SV, Shivashankar BS, Mulik VK, Prajapati PM, Ganesh Sanjeev, Sharma SC, Bhagwat PV, Mohanty AK, Ganesan S, Goswami A (2012) Measurement of the ^{232}Th(n, γ)^{233}Th and ^{232}Th(n, 2n)^{231}Th reaction cross- sections at neutron energies of 8.04 $\pm$ 0.30 and 11.90 $\pm$ 0.35 MeV. Ann Nucl Energy 47:160
12. Mukerji S, Naik H, Suryanarayana SV, Chachara S, Shivashankar BS, Mulik V, Sharma SC (2012) Measurement of ^{232}Th(n, γ) and ^{232}Th(n, 2n) cross-sections at neutron energies of 13.5, 15.5 and 17.28 MeV using neutron activation techniques. Pramana 79(2):249–262
13. Naik H, Surayanarayana SV, Bishnoi S, Patel T, Sinha A, Goswami A (2015) Neutron induced reaction cross-section of ^{232}Th and ^{238}U at the neutron energies of 2.45 and 14.8 MeV. J Radioanal Nucl Chem 303(3):2497–2504
14. Zysin YA, Kovrizhnykh AA, Lbov AA, Selchenkov LI (1961) Cross section for the reaction ^{232}Th(n, 2n)^{231}Th at 14.7 Mev neutron energy. At Energ 8(4):310
15. Reyhancan IA (2011) Measurements and model calculations of activation cross sections for ^{232}Th (n, 2n)^{231}Th reaction between 13.57 and 14.83 MeV neutrons. Ann Nucl Energy 38(11):2359–2362
16. Raics P, Nagy S, Daroczy S, Komilov NV (1990) Indo International Nuclear Data Committee
17. Phillips JA (1958) The (n, 2n) cross-section of ^{232}Th for fission neutrons. J Nucl Eng 7(3–4):215–219
18. Perkin JL, Coleman RF (1961) Cross-sections for the (n, 2n) reactions of ^{232}Th, ^{238}U and ^{237}Np with 14 MeV neutrons. J Nucl Energy Parts A/B React Sci Technol 14(1–4):69–75
19. Ikeda Y, Konno C, Oishi K, Nakamura T, Miyade H, Kawade K, Katoh T (1988) Activation cross section measurements for fusion reactor structural materials at neutron energy from 13.3 to 15.0 MeV using FNS facility (No. JAERI–1312). Japan Atomic Energy Research Institute
20. Kobayashi K, Hashimoto T, Kimura I (1971) Measurements of Average Cross Section for ^{232}Th(n, 2n)^{231}Th Reaction to Neutrons with Fission-Type Reactor Spectrum and of Gamma-Ray Intensities of ^{231}Th. J Nucl Sci Technol 8(9):492–497
21. Karius H, Ackermann A, Scobel W (1979) The pre-equilibrium contribution to the (n, 2n) reactions of ^{232}Th and ^{238}U. J Phys G Nucl Phys 5(5):715
22. Karamanis D, Andriamonje S, Assimakopoulos PA, Doukellis G, Karademos DA, Karydas A, Papadopoulos CT (2003) Neutron cross-section measurements in the Th–U cycle by the activation method. Nucl Instrum Methods Phys Res Sect A 505(1–2):381–384
23. Filatenkov AA (2016) Neutron activation cross sections measured at KRI in neutron energy region 13.4–14.9 MeV. Report, USSR report to the INDC (0460)
24. Chatani H, Kimura I (1992) Measurement of the ^{232}Th(n, 2n)^{231}Th reaction cross section with 14.5 MeV neutrons. Ann Nucl Energy 19(8):425–429
25. Konno C (1993) Activation cross section measurements at neutron energy from 13.3 to 15.0 MeV using the FNS facility. JAERI1329
26. Chatani H (1983) A Measurement of the Averaged cross Section for the ^{232}Th(n, 2n)^{231}Th Reaction with a Fission Plate. Nucl Instrum Methods Phys Res 205(3):501–504
27. Butler JP, Santry DC (1961) ^{232}Th(n, 2n)^{231}Th cross section from threshold to 20.4 MeV. Can J Chem 39(3):689–696
28. Shivashankar BS, Ganesan S, Naik H, Suryanarayana SV, Nair NS, Prasad KM (2015) Measurement and covariance analysis of reaction cross sections for ^{58}Ni(n, p)^{58}Co relative to cross section for formation of ^{97}Zr fission product in neutron-induced fission of ^{232}Th and ^{238}U at effective neutron energies E_n = 5.89, 10.11, and 15.87 MeV. Nucl Sci Eng 179(4):423–433
29. Yerraguntla SS, Naik H, Karantha MP, Ganesan S, Suryanarayana SV, Badwar S (2017) Measurement of ^{59}Co(n, γ)^{60}Co reaction cross sections at the effective neutron energies of 11.98 and 15.75 MeV. J Radioanal Nucl Chem 314(1):457–465
30. Ganesan S (2015) Nuclear data covariances in the indian context-progress, challenges, excitement and perspectives. Nucl Data Sheets 123:21–26
31. Meghna RK, Naik H, Sripathi PK, Manjunatha PK, Yerraguntla SS, Ganesan S, Suryanarayana SV (2018) Detailed data sets related to measurement and covariance analysis of ^{232}Th(n, 2n)^{231}Th reaction cross section. https://doi.org/10.13140/RG.2.2.18415.69282
32. Ziegler JF (2016) SRIM-2013. The stopping and Range of Ions in Solids. Pergamon, New York, p 2013
33. Makwana R, Mukherjee S, Mishra P, Naik H, Singh NL, Mehta M, Yerraguntla Santhi Sheela, Karkera M (2017) Measurements of the cross sections of the ^{189}W(n, γ)^{187}W, ^{182}W(n, p)^{182}Ta,

^{154}Gd(n, 2 n)^{153}Gd, and ^{160}Gd(n, 2 n)^{159}Gd reactions at neutron energies of 5 to 17 MeV. Phys Rev C 96(2):024608
34. Poppe CH, Anderson JD, Davis JC, Grimes SM, Wong C (1976) Cross sections for the ^{7}Li(p, n)^{7}Be reaction between 4.2 and 26 MeV. Phys Rev C 14(2):438
35. Smith DL, Plompen AJM, Semkova V (2005) Correction for low energy neutrons by spectral indexing. Neutron Activation Cross-Section Measurements from Threshold to 20 MeV
36. Millsap DW, Landsberger S (2015) Self-attenuation as a function of gamma ray energy in naturally occurring radioactive material in the oil and gas industry. Appl Radiat Isot 97:21–23
37. Nowotny R (1998) XMuDat: photon attenuation data on PC. IAEA Report IAEA-NDS 195. https://www-nds.iaea.org/publications/iaea-nds/iaea-nds-0195.htm
38. Vidmar T (2005) EFFTRAN—a Monte Carlo efficiency transfer code for gamma-ray spectrometry. Nucl Instrum Methods Phys Res Sect A 550(3):603–608
39. Sonzogni A (2017) NuDat 2.6 (as of April 17, 2017), National Nuclear Data Center, Brookhaven National Laboratory. https://www.nndc.bnl.gov/
40. Blons J, Mazur C, Paya D (1975) Evidence for rotational bands near the ^{232}Th(n, f) fission threshold. Phys Rev Lett 35(26):1749
41. Glendenin LE, Gindler JE, Ahmad I, Henderson DJ, Meadows JW (1980) Mass distributions in monoenergetic-neutron-induced fission of ^{232}Th. Phys Rev C 22(1):152
42. Borchers RR, Poppe CH (1963) Neutrons from proton bombardment of lithium. Phys Rev 129(6):2679
43. Santhi Sheela, Naik H, Prasad KM, Ganesan S, Nair NS, Suryanarayana SV (2017) Covariance analysis of efficiency calibration of HPGe detector. Internal Report, No. MU/STATISTICS/DAE-BRNS/2017/1, 19-February-2017, https://doi.org/10.13140/rg.2.2.32025.21605
44. Chadwick M, Herman M, Oblozinsky P, Dunn ME, Danon Y, Kahler A, Smith DL, Pritychenko B, Arbanas G, Arcilla R, Brewer R, Brown DA, Capote R, Carlson AD, Cho YS, Derrien H, Guber K, Hale GM, Hoblit S, Holloway S, Johnson TD, Kawano T, Kiedrowski BC, Kim H, Kunieda S, Larson NM, Leal L, Lestone JP, Little RC, McCutchan EA, MacFarlane RE, MacInnes M, Mattoon CM, McKnight RD, Mughabghab SF, Nobre GPA, Palmiotti G, Palumbo A, Pigni MT, Pronyaev VG, Sayer RO, Sonzogni AA, Summers NC, Talou P, Thompson IJ, Trkov A, Vogt RL, van der Marck SC, Wallner A, White MC, Wiarda D, Young PG (2011) ENDF/B-VII.1 nuclear data for science and technology: cross sections. Covariances, fission prod yields decay data. Nucl Data Sheets 112:2887–2996
45. Shibata K, Iwamoto O, Nakagawa T, Iwamoto N, Ichihara A, Kunieda S, Chiba S, Furutaka K, Otuka N, Ohasawa T, Murata T, Matsunobu H, Zukeran A, Kamada S, Katakura J (2011) JENDL-4.0: a new library for nuclear science and engineering. J Nucl Sci Technol 48:1–30
46. Koning AJ, Bauge E, Dean CJ, Dupont E, Fischer U, Forrest RA, Jacqmin R, Leeb H, Kellett MA, Mills RW, Nordborg CM, Pescarini Rugama Y, Rullhusen P (2011) Status of the JEFF nuclear data library. J Korean Phys Soc 59(2):1057–1062
47. Zabrodskaya SV, Ignatyuk AV, Koscheev VN (2007) ROSFOND-Rossiyskaya Natsionalnaya Biblioteka Nejtronnykh Dannykh. In: VANT, nuclear constants, pp 1–2
48. Koning AJ, Hilaire S, Goriely S (2015) TALYS User Manual: A Nuclear Reaction Program (Westerduinweg 3, P.O. Box 25, NL-1755 ZG Prtten, The Netherlands, 2015). http://www.talys.eu/download-talys/